74% of the cell density in the 10% FCS medium throughout.

## Effects of fish serum concentration on cell growth and hGM-CSF production

To investigate the effects of fish serum concentration on cell growth and hGM-CSF production, the medium was changed to fish serum (0–30%) medium at 24 h after the inoculation with 10% FCS medium (Fig. 2). Twenty percent fish serum gave the highest cell density at 72 h among the tested fish serum concentrations, and the cell density was 75% that in the 10% FCS medium throughout. The specific production rate of hGM-CSF in the 20% fish serum medium was the highest among those in the fish serum media and was 64% that in the 10% FCS medium.

## Effects of fish serum on cell adhesion to and growth on collagen-coated dishes

To study the effect of fish serum on cell adhesion to collagen-coated dishes, CHO cells were inoculated onto normal culture and collagen-coated dishes with several media containing 10% FCS or fish serum, and the density of adhering cells was determined after 24 h (Fig. 3). The cell densities in the 10% FCS medium were highest among those in several media on both dishes, and the adhesion rates were 138 and 112% on the normal culture and collagen-coated dishes, respectively. The cell densities in the fish serum media (0–30%) on the normal culture dishes were very low, and the adhesion rates in such media were less than 35%. The cell densities in the fish serum media on the collagen-coated dishes depended on the concentration of fish serum, and 20% fish serum gave the highest cell density of $1.5\times10^4$ cells/cm$^2$, for which the adhesion rate was 91%.

To investigate the effect of fish serum on the growth of CHO cells on collagen-coated dishes, the cells were inoculated into 10% FCS or 20% fish serum medium, and the medium was changed to 20% fish serum or serum-free medium after 24 h (Fig. 4). The cell density at 72 h ($4.2\times10^4$ cells/cm$^2$) in the 20% fish serum medium was markedly higher than that in the culture in which the medium was changed from 20% fish serum medium to serum-free medium. The growth rate (24–72 h) in the 20% fish serum medium was almost the same as that in the culture in which the medium was changed from 10% FCS medium to 20% fish serum medium, whereas the growth rate in the 10% FCS medium was higher than that in the culture in which the medium was changed from 10% FCS medium to 20% fish serum medium.

## hGM-CSF production on collagen-coated dishes

The specific production rate of hGM-CSF during culture for 72 h on collagen-coated dishes using 10% FCS or 20% fish serum was determined (Table 1). There was no marked

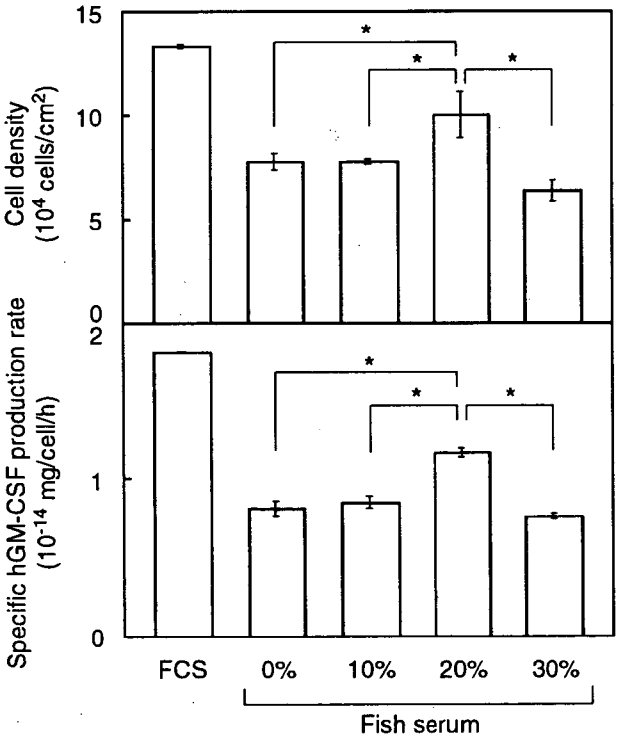


Fig. 2 Effects of concentration of fish serum on cell growth and hGM-CSF production. CHO DR1000L4N cells were cultivated for 72 h on medium containing 0, 10, 20, or 30% fish serum or 10% FCS after cultivation for 24 h on 10% FCS medium. Data represent mean± SD ($n$=3); *asterisks*: $P<0.05$

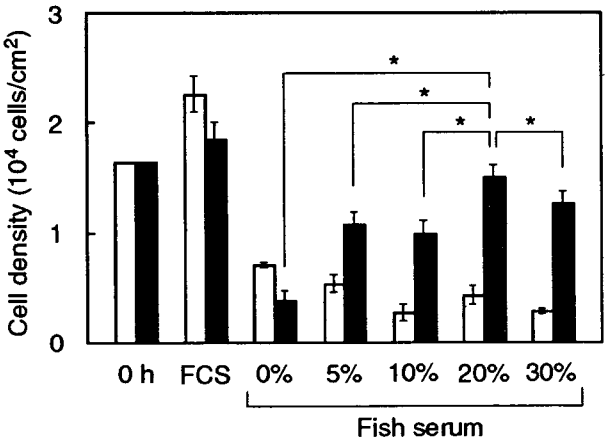


Fig. 3 Effect of fish serum on adhesion of CHO cells on collagen-coated dishes. CHO DR1000L4N cells were inoculated onto several media containing 10% FCS or fish serum (0–30%) on normal culture (*open bars*) and type I collagen-coated (*closed bars*) dishes. Density of adhering cells was determined after 24 h. Data represent mean±SD ($n$=3); *asterisk*: $P<0.05$

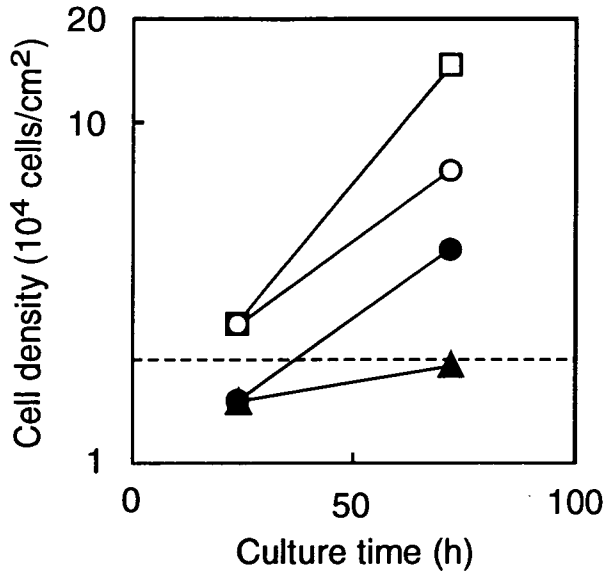


**Fig. 4** Effect of fish serum on cell growth on collagen-coated dishes. CHO DR1000L4N cells were inoculated onto collagen-coated dishes with media containing 10% FCS (*open squares*, *open circles*) or 20% fish serum (*filled circles*, *filled triangles*). The medium was changed to 20% fish serum medium (*open circles*) or serum-free medium (*filled triangles*) at 24 h. A *dashed line* represents the level of inoculum cell density ($2.0\times10^4$ cells/cm$^2$). Data represent the mean of triplicate cultures

difference between the specific production rates of hGM-CSF in the media with 20% fish serum and 10% FCS.

## Discussion

As there should be no report that fish serum is employed for mammalian cell culture, the effects of fish serum on the adhesion and growth of CHO cells were compared with those of FCS in this study. The density of adhering cells after 24-h incubation in the serum-free medium was only 57% that in the 10% FCS medium (Fig. 1). The density of adhering cells after 24-h incubation in the 10% fish serum medium was even lower than that in the serum-free medium. Thus, fish serum may inhibit cell adhesion on culture dishes. However, fish serum stimulated cell adhesion on the collagen-coated dishes (Fig. 3). The reason for the inhibitory effect of fish serum on cell adhesion is still unclear and whether this characteristic is common to other fish sera than *Pagrus major* serum should be studied in the future.

After cell adhesion to the culture dishes with the 10% FCS medium, the cell density in the 10% fish serum medium increased until 72 h and thereafter remained constant (Fig. 1). This time course of cell density was analogous to that of cell density in the 10% FCS medium. However, the concentration of 10% for fish serum should not be enough to stimulate cell growth as shown in Fig. 2. On the other hand, the cell density in the 20% fish serum medium after initial adhesion in the 10% FCS medium on the culture dishes was markedly higher than those for 0 and 10% fish serum media and reached 75% that in the 10% FCS medium (Fig. 2). Therefore, the promotion of cell growth needed the concentration of 20% for fish serum. The average cell-doubling time in the 20% fish serum medium on the collagen-coated dishes (33 h) was comparable to that in the 10% FCS medium (19 h; Fig. 4). Consequently, the growth-stimulating activity of serum from *Pagrus major* might not be markedly high but is sufficient for CHO cells.

The specific hGM-CSF production rate of cells grown in the 20% fish serum medium after initial adhesion in the 10% FCS medium was 64% that of cells grown in the 10% FCS medium (Fig. 2). Moreover, the cells harvested on the collagen-coated dishes with the 20% fish serum medium throughout entire culture period showed almost the same specific production rate of hGM-CSF as the cells cultivated in the 10% FCS medium (Table 1). Furthermore, there was no apparent difference in the morphology of the CHO cells observed under a phase contrast microscope between the cells cultivated in the fish serum medium and those cultivated in the FCS medium (data not shown). Thus, there may be no difference in cell quality in practical hGM-CSF production between the cells grown in the medium containing fish serum and those grown in the medium containing FCS.

The cell growth and hGM-CSF production of cells after initial adhesion in the 10% FCS medium on the culture dishes (Fig. 2) and cell adhesion to the collagen-coated dishes (Fig. 3) were maximum at the same concentration of fish serum (20%). Thus, this concentration (20%) may be suboptimum for the effect of serum from *Pagrus major*. The suboptimum concentration of 20% for fish serum was indeed higher than the common concentration of 10% for FCS. The cost of 20% fish serum medium should be compared with that of 10% FCS medium when the price of fish serum is decided in the future.

**Table 1** Specific production rates of hGM-CSF for CHO cells cultivated on collagen-coated dishes

| Serum[a] | Specific production rate of hGM-CSF[b] ($10^{-13}$ mg cell$^{-1}$ h$^{-1}$) |
|---|---|
| Fish serum (20%) | 1.26±0.31 |
| FCS (10%) | 1.21±0.32 |

[a] CHO DR1000L4N cells were inoculated onto collagen-coated dishes containing 10% FCS medium and 20% fish serum medium and cultivated for 72 h.

[b] Data represent mean±SD ($n$=3)

In this study, although serum from *Pagrus major* inhibited the initial adhesion of CHO cells to the culture dishes, its stimulatory effect on cell growth after cell adhesion with FCS was comparable with that of FCS. And it stimulated cell adhesion to and cell growth on the collagen-coated dishes. Thus, fish serum should be utilized instead of FCS in large-scale microcarrier culture with collagen microcarriers such as Cytodex 3. The application of fish serum to suspension culture should be investigated in the future.

## References


Funkenstein B, Silgergeld A, Cavari B, Laron Z (1989) Growth hormone increases plasma levels of insulin-like growth factor (IGF-I) in a teleost, the gilthead seabream (*Sparus aurata*). J Endocrinol 120:R19–R21

Hata J-i, Takeo J, Segawa C, Yamashita S (1997) A cDNA encoding fish fibroblast growth factor-2, which lacks alternative translation initiation. J Biol Chem 272:7285–7289

Larsen DA, Beckman BR, Dickhoff WW (2001) The effect of low temperature and fasting during the winter on metabolic stores and endocrine physiology (insulin, insulin-like growth factor-I, and thyroxine) of coho salmon, *Oncorhynchus kisutch*. Gen Comp Endocrinol 123:308–323

Nordgarden U, Hansen T, Hemre G-I, Sundby A, Björnsson BT (2005) Endocrine growth regulation of adult atlantic salmon in seawater: the effect of light regime on plasma growth hormone, insulin-like growth factor-I, and insulin levels. Aquaculture 250:862–871

Rathore G, Sood N, Swaminathan R (2001) Primary cell culture from fish gills and kidney using fish serum. Indian J Exp Biol 39:936–938

Sanford KK, Earle WR, Evans VJ, Walts HK, Shannon JE (1951) The measurement of proliferation in tissue cultures by enumeration of cell nuclei. J Natl Cancer Inst 11:773–795

Small BC, Peterson BC (2005) Establishment of a time-resolved fluoroimmunoassay for measuring plasma insulin-like growth factor I (IGF-I) in fish: effect of fasting on plasma concentrations and tissue mRNA expression of IGF-I and growth hormone (GH) in channel catfish (*Ictalurus punctatus*). Domest Anim Endocrinol 28:202–215

Suzuki T, Kurokawa T, Asashima M (1994) Identification of a heparin-binding, mesoderm-inducing peptide in the swim-bladder of the red seabream, *Pagrus major*: a probable fish fibroblast growth factor. Fish Physiol Biochem 13:343–352

Yoshikawa T, Nakanishi F, Ogura Y, Oi D, Omasa T, Katakura Y, Kishimoto M, Suga K (2000) Amplified gene location in chromosomal DNA affected recombinant protein production and stability of amplified genes. Biotechnol Prog 16:710–715

Yoshimizu M, Kasai H (2005) Frontiers of viral disease in fish: current situation and preventive measures. Kagaku to Seibutsu 43:48–58 (in Japanese)

Journal of Biomedical Optics 12(5), 054010 (September/October 2007)

# Noninvasive measurement of three-dimensional morphology of adhered animal cells employing phase-shifting laser microscope

**Mutsumi Takagi**
**Takayuki Kitabayashi**
**Syunsuke Ito**
**Masashi Fujiwara**
Hokkaido University
Graduate School of Engineering
Division of Biotechnology and Macromolecular Chemistry
Sapporo 060-8628, Japan
E-mail: takagi-m@eng.hokudai.ac.jp

**Akio Tokuda**
FK Optical Laboratory
1-13-4 Nakano, Ni-iza
Saitama 352-0005, Japan

**Abstract.** Noninvasive measurement of 3-D morphology of adhered animal cells employing a phase-shifting laser microscope (PLM) is investigated, in which the phase shift for each pixel in the view field caused by cell height and the difference in refractive indices between the cells and the medium is determined. By employing saline with different refractive indices instead of a culture medium, the refractive index of the cells, which is necessary for the determination of cell height, is determined under PLM. The observed height of Chinese hamster ovary (CHO) cells cultivated under higher osmolarity is lower than that of the cells cultivated under physiological osmolarity, which is in agreement with previous data observed under an atomic force microscope (AFM). Maximum heights of human bone marrow mesenchymal stem cells and human umbilical cord vein endothelial cells measured under PLM and AFM agree well with each other. The maximum height of nonadherent spherical CHO cells observed under PLM is comparable to the cell diameter measured under a phase contrast inverted microscope. Laser irradiation, which is necessary for the observation under PLM, did not affect 3-D cell morphology. In conclusion, 3-D morphology of adhered animal cells can be noninvasively measured under PLM.  [DOI: 10.1117/1.2779350]

Keywords: morphology; noninvasive; three dimensional; laser microscope.

Paper 06215R received Aug. 8, 2006; revised manuscript received Mar. 19, 2007; accepted for publication May 15, 2007; published online Sep. 12, 2007.

## 1 Introduction

Animal cell cultivation is a very important technology for pharmaceutical production and cell processing for regenerative medicine. To optimize and control the quality of cells during cultivation, monitoring of cell quantity and quality can be carried out nondestructively and noninvasively, especially in cell processing for transplantation and regenerative medicine. Although light microscopic observation is useful for the noninvasive monitoring of adhered animal cells, this technique cannot facilitate 3-D morphological observation, but only 2-D morphological observation.

An atomic force microscope (AFM) can be used to observe the 3-D morphology of adhered animal cells. For example, the differences in 3-D morphology between Chinese hamster ovary (CHO) cells cultivated under various osmolarities were measured under AFM after fixation treatment of cells.[1] Because 3-D observation of adhered animal cells using AFM requires a long time and fixing treatment of cells, AFM observation is considered invasive for cells.

Recently, a novel phase-shifting laser microscope (PLM) was developed.[2] A biprism, located between the magnifying lens and the observation plane, was used as a beamsplitter. (Fig. 1) The biprism was laterally translated to introduce phase shifts required for quantitative phase measurement with a phase-shifting technique. Namely, the phase shift ($\Delta\Phi$) caused by the difference in refractive indices between the sample and the reference expressed in Eq. (1) can be determined using PLM.

$$\Delta\Phi = 2\pi d \times \frac{n_1 - n_0}{\lambda_0}, \tag{1}$$

where $\Delta\Phi$ is the phase shift (-); $d$ is the thickness of the sample (nanometers); $\lambda_0$ is the wavelength of the laser (nm); and $n_1$ and $n_0$ are the refractive indices of the sample and reference (-), respectively. We believe that PLM may be applicable for measuring the thickness ($d$) of living adhered cells by substituting the refractive indices of cells and the medium to $n_1$ and $n_0$ in Eq. (1), respectively.

In this study, noninvasive 3-D observation of animal cells under PLM without fixing treatment was investigated.

Address all correspondence to Mutsumi Takagi, Graduate School of Engineering Hokkaido University N13, W8 - Sapporo, Hokkaido 060-8628 Japan; Tel: +81-11-706-6567; Fax: +81-11-706-6567; E-mail: takagi-m@eng.hokudai.ac.jp

1083-3668/2007/12(5)/054010/5/$25.00 © 2007 SPIE

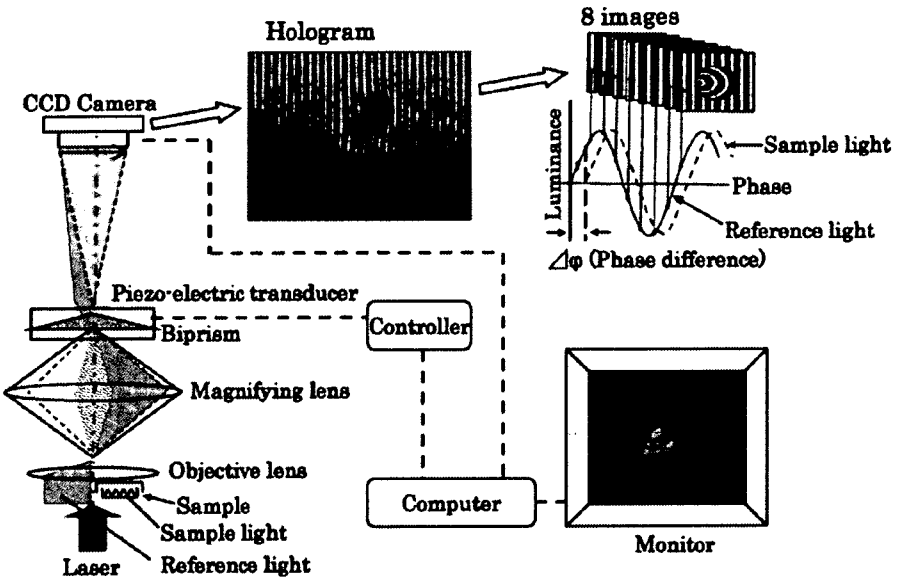


Fig. 1 Schematic diagram of phase-shifting laser microscope.

## 2 Materials and Methods

### 2.1 *Cells and Media*

Tissue plasminogen activator (tPA)-producing Chinese hamster ovary (CHO) 1-15500 cells (ATCC CRL-9606) were used. Ham's F-12K medium (Dainippon Seiyaku Company, Limited, Japan) supplemented with 10% newborn bovine serum (NBS, Gibco, New York), streptomycin (0.1 mg/L), and penicillin (100 u/L) was employed for cell growth. Medium osmolarity was adjusted to 300 and 400 mOsm/L by the addition of NaCl solution (100 g/L). Medium osmolarity was determined by measuring the depression of the freezing point using an osmometer (model OM-801, Vogel, Germany). CHO cells ($6.7\times10^4$ cells) were inoculated into 2 ml of the medium in a dish (Falcon, 9.6 $cm^2$) and incubated for 4 d in a $CO_2$ incubator (37°C, 5% $CO_2$). Cell suspension was prepared by trypsinization of adhered cells on a dish.

Human bone marrow mesenchymal stem cells (MSCs) were isolated from bone marrow aspirate obtained by routine iliac crest aspiration from human donors (age 65 to 73) as previously reported.[3] The content of $CD105^+$ $CD45^-$ cells among the cells analyzed by a flowcytometer was approximately 90% (data not shown).[4] MSCs were cultured at densities of $0.15\times10^4$ cells/$cm^2$ employing DMEM-LG (Gibco, New York) supplemented with 10% Fetal Calf Serum (FCS) (Gibco), 2500 U/l penicillin, and 2.5 mg/l streptomycin.

Human umbilical cord vein endothelial cells (HUVEC) were purchased from Cambrex Bio Science Walkersville, Incorporated (Maryland) and cultured at densities of $0.2\times10^4$ cells/$cm^2$ employing DMEM (Gibco, Japan) supplemented with 10% inactivated fetal bovine serum (Gibco), 1 aliquot (of the same concentration as that in MEM) of MEM nonessential amino acids (Gibco), 2-mM glutamine, 5000 U/L penicillin, and 5 mg/L streptomycin (Sigma, Missouri).

### 2.2 *Cell Morphology Analysis under Phase-Shifting Laser Microscope*

The adhered cells on the bottom surface of the culture dish were observed under PLM. Two neighboring fields of view with cells and without cells were selected as sample and reference fields, respectively, and phase shift ($\Delta\Phi$) was determined for all pixels in the sample field under PLM. By substituting the wavelength of the laser ($\lambda_0$=632.8 nm), the refractive indices of the cells determined by the method mentioned later ($n_1$=1.39, 1.375, and 1.375 for CHO, MSC, and HUVEC, respectively) and the medium ($n_0$=1.34), and the measured phase shift ($\Delta\Phi$) to Eq. (2), the height of the cells ($d$ nm) was calculated for all pixels in the sample field, and a 3-D view of the sample field was made.

$$d=\frac{\Delta\Phi}{2\pi}\times\frac{\lambda_0}{n_1-n_0} \tag{2}$$

### 2.3 *Determination of Refractive Index of Cells*

The culture medium was replaced with saline containing different concentrations of bovine serum albumin (380 to 480 g/L), in which osmolarity was adjusted to the original medium osmolarity, and cells were observed under PLM. The refractive index of the saline, with which cell images disapperared under PLM, was considered as the refractive index of the cells. The refractive indices of the medium and saline were determined using a refract meter (DR-A1, Atago Company, Tokyo, Japan).

### 2.4 *Cell Observation under Atomic Force Microscope*

Cells were fixed with glutaraldehyde (4%), dried, and analyzed using an atomic force microscope (AFM)(NanoScope

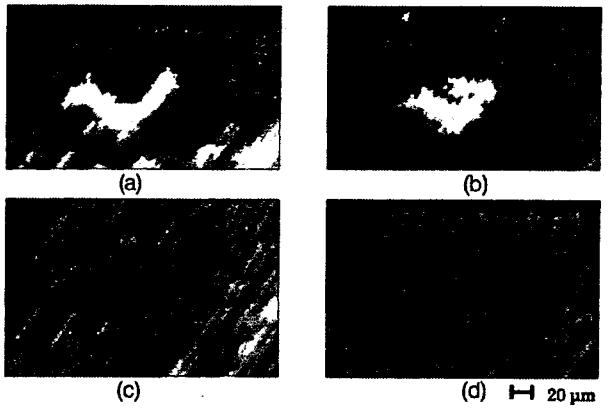


Fig. 2 Determination of refractive index of adhered CHO cells. CHO cells adhered to a culture dish containing saline with known refractive indices (a) 1.33, (b) 1.34, (c) 1.38, and (d) 1.39 were observed under PLM. The color bar is analogous to that in Fig. 3.

IIIa, Veeco). Namely, the height was scanned for all parts of each cell, and the closed area showing positive height was defined as the cell adhesive area.[5]

## 3 Results and Discussion

### 3.1 *Determination of Refractive Index of Adhered Chinese Hamster Ovary Cells*

After the CHO cells in the culture medium were observed under PLM, the culture medium was replaced with saline containing albumin while the culture dish was fixed on the stage of PLM. Cell image was distinct with the saline, having refractive indices of 1.33 and 1.34 (Fig. 2). Cell image was indistinct for the saline refractive index of 1.38 and was not observed for the saline refractive index of 1.39. Consequently, the refractive index of the observed CHO cells was determined to be 1.39.

The refractive index of the cell membrane (1.5) is higher than that of the cytoplasm (1.35),[6] and the thickness of the cell membrane is approximately 7.5 nm.[7] Because the adopted refractive index for CHO cells in this study (1.39) was between 1.35 and 1.5, it may be the sum of the refractive indices of the cell membrane and cytoplasm. However, the digit of significant figures must increase to increase the accuracy of the cell height measurement under PLM in the future, because the difference in refractive index between the cells and the medium was small (e.g., 0.05).

### 3.2 *Effect of Osmolarity on Three-Dimensional Cell Morphology Observed under Phase-Shifting Laser Microscope*

CHO cells cultivated for 4 *d* under different osmolarities of 300 and 400 mOsm/L were observed under PLM [Figs. 3(a) and 3(b)]. The 2-D morphology of the CHO cells cultivated under 400 mOsm/L was elongated, while that of the CHO cells cultivated under 300 mOsm/L was globular. This difference in the 2-D cell morphology between the CHO cells cultivated under different osmolarities is in agreement with previous observations not only under AFM, but also under a conventional light-inverted microscope.[1]

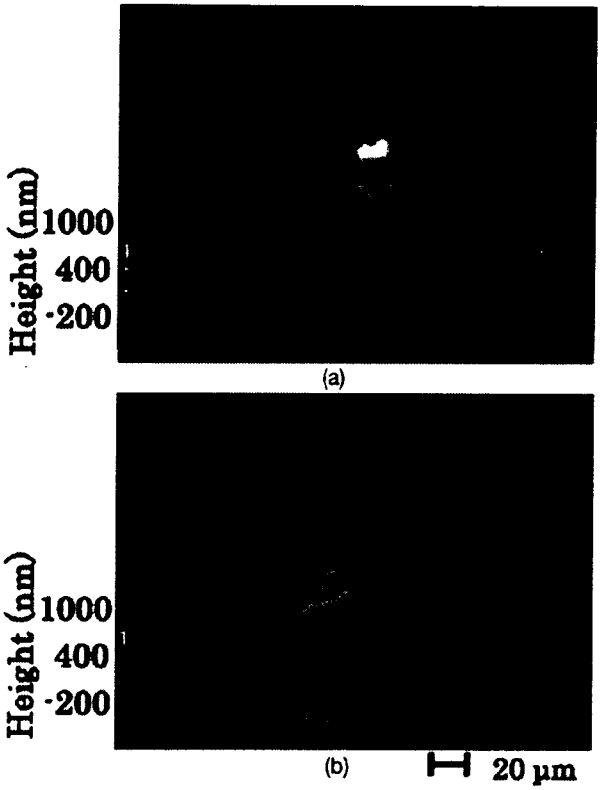


Fig. 3 Observation of CHO cells cultivated under different osmolarities under PLM. 3-D views of CHO cells cultivated under (a) 300 and (b) 400 mOsm/L.

The height of the CHO cells cultivated under 400 mOsm/L [Fig. 3(b)] was lower than that of the CHO cells cultivated under 300 mOsm/L [Fig. 3(a)]. The comparison of the average value for each ten cells showed that the cell maximum height under 400 mOsm/L was apparently lower than that under 300 mOsm/L (Fig. 4). This dependency of cell height on osmolarity is in agreement with a previous report observed under AFM.[1] Moreover, there was no marked difference between the measured values under PLM and AFM

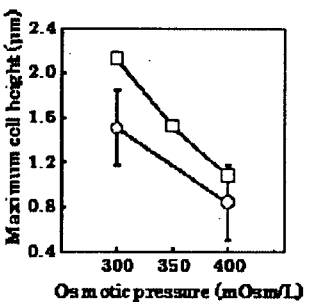


Fig. 4 Effect of osmolarities on maximum cell height. The maximum height of each cell ($n$=10, mean±SD) observed under PLM (circle) was plotted against osmolarity together with that of each cell observed under AFM (square).

**Table 1** Cell maximum height measurement under PLM and AFM. The maximum height of each cell ($n$=10, mean±SD) observed under PLM and AFM are shown.

| Cell species | Cell maximum height ($\mu$m) | |
|---|---|---|
| | PLM | AFM |
| CHO | 2.00±0.92 | 2.06±0.63 |
| MSC | 1.52±0.79 | 1.73±0.46 |
| HUVEC | 1.09±0.92 | 1.20±0.30 |

(Fig. 4). These results strongly suggest the accuracy of cell height measurement using PLM.

### 3.3 *Comparison of Maximum Cell Heights Measured by Phase-Shifting Laser Microscope and Atomic Force Microscope for Various Cell Species*

To confirm the accuracy of measured cell height under PLM and the applicability of PLM to various kinds of animal cells, adhesive CHO, MSC, and HUVEC cells were observed under PLM without fixation and AFM with fixation and drying (Table 1). Average cell height of CHO cells was higher than those of MSC and HUVEC in both measurements of PLM and AFM. Average cell height of MSC cells were between those of CHO and HUVEC in both measurements of PLM and AFM. Average cell heights measured by PLM were near to those measured by AFM in all cell kinds, while the standard deviations for PLM measurement were a little larger than those for AFM measurement. These data can show that the accuracy of cell height measurement by PLM and PLM measurement should be applicable to various cell species.

### 3.4 *Comparison of Maximum Height Measured by Phase-Shifting Microscope and Two-Dimensional Diameter for Nonadherent Spherical Chinese Hamster Ovary Cells*

To confirm the accuracy of maximum cell height measure by PLM, maximum cell height of nonadherent spherical CHO cells measured by PLM was compared with their horizontal diameter measured by PLM or conventional inverted microscope. Nonadherent CHO cells were prepared by tripsinization of adherent cells and measured in medium (Table 2). There was no marked difference in the horizontal diameter of cells between PLM (7.33±1.49) and inverted microscope (8.78±1.20) measurements. Cell maximum height measured by PLM (5.68±2.53) was comparable to cell diameters. Cell

**Table 2** Observation of nonadherent CHO cells under PLM. Diameter and maximum height of nonadherent spherical CHO cells were measured by the observation under PLM and inverted phase contrast microscope. Mean±SD ($n$=10) are shown.

| Cell maximum height ($\mu$m) | Cell diameter ($\mu$m) | |
|---|---|---|
| PLM | PLM | Inverted microscope |
| 5.68±2.53 | 7.33±1.49 | 8.78±1.20 |

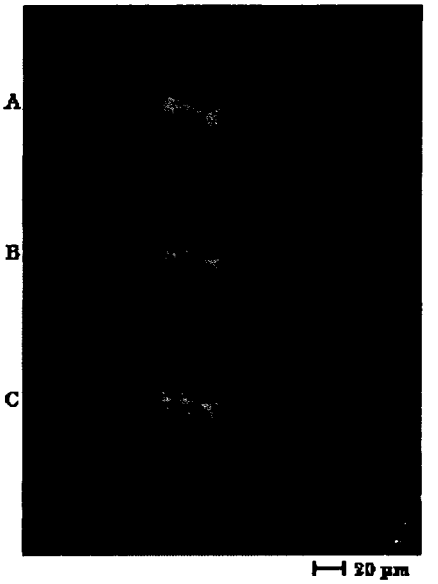


**Fig. 5** Influence of laser irradiation on 3-D cell morphology of CHO cells. The time lengths of laser irradiation for CHO cells before observation under PLM were (a) 0, (b) 5, and (c) 10 min, respectively. The color bar is analogous to that in Fig. 3 (color online only).

maximum height (5.68±2.53) measured by PLM was smaller than the horizontal diameter (7.33±1.49) measured by PLM. This shows that cell height was a little smaller than the horizontal diameter due to the gravity force. These data support the accuracy of cell height measurement by PLM.

### 3.5 *Influence of Laser Irradiation on Cell Morphology*

To confirm the influence of laser irradiation required for PLM observation on cell morphology, a dish containing adhered CHO cells was set on the stage of a PLM and received continuous irradiation of a laser for 10 min, during which a 3-D cell morphology was observed at 0, 5, and 10 min, respectively (Fig. 5). There was no marked change in the 3-D cell morphology of the CHO cells during the laser irradiation for 10 min.

The laser irradiation dose required for PLM observation was less than 0.1 mW, and may not influence 3-D cell morphology, because an observation of one sample under PLM took only 30 s.

The spatial resolution in cell height observed under PLM should be approximately 10 to 2 nm, because the resolution in phase shift is 10 to 5 rad and the difference in refractive index between cell and medium is 0.04. This resolution under PLM might be comparable with or better than that observed under AFM. Cells adhered on the bottom of a conventional culture dish can be observed under PLM *in situ* together with culture medium, while cells need to attach onto some special board and liquid culture medium should be removed for observation under AFM. So, PLM observation might be noninvasive compared to AFM observation. Observation of cells under PLM takes only a few minutes and needs no special training, because 3-D morphology can be observed for voluntary cells selected under a normal light inverted microscope. Moreover,

there is almost no restriction for cell height observed under PLM, while cell height observed under AFM is limited by the size of the lever (e.g., 5 $\mu$m). Consequently, the observation of 3-D cell morphology under PLM might be more attractive for academic and pharmaceutical research compared to AFM observation.

## 4 Conclusion

These data show that PLM can quantitatively measure the 3-D morphology of adhesive animal cells noninvasively.

### References


1. M. Takagi, H. Hayashi, and T. Yoshida, "The effect of osmolarity on metabolism and morphology in adhesion and suspension Chinese hamster ovary cells producing tissue plasminogen activator," *Cytotechnology* **32**, 171–179 (2000).
2. J. Endo, J. Chen, D. Kobayashi, Y. Wada, and H. Fujita, "Transmission laser microscope using the phase-shifting technique and its application to measurement of optical waveguides," *Appl. Opt.* **41**(7), 1308–1314 (2002).
3. C. Matsuda, M. Takagi, T. Hattori, S. Wakitani, and T. Yoshida, "Differentiation of human bone marrow mesenchymal stem cells to chondrocytes for construction of three-dimensional cartilage tissue," *Cytotechnology* **47**, 11–17 (2005).
4. M. Takagi, T. Nakamura, C. Matsuda, T. Hattori, S. Wakitani, and T. Yoshida, "In vitro proliferation of human bone marrow mesenchymal stem cells employing donor serum and basic fibroblast growth factor," *Cytotechnology* **43**(1-3), 89–96 (2003)
5. H. J. Butt, E. K. Wolff, S. A. Gould, N. B. Dixon, C. M. Peterson, and P. K. Hansma, "Imaging cells with the atomic force microscope," *J. Struct. Biol.* **105**, 54–61 (1990).
6. J. Sonke and A. W. Edith, "The physical basis of transparency in biological tissue: Ultrastructure and minimization of light scattering," *J. Theor. Biol.* **199**, 181–198 (1999).
7. A. M. Richard, "Light scattering from biological cells: dependence of backscatter radiation on membrane thickness and refractive index," *Appl. Opt.* **18**(5), 585–588 (1979).

JOURNAL OF BIOSCIENCE AND BIOENGINEERING
Vol. 104, No. 6, 510–512. 2007
DOI: 10.1263/jbb.104.510



# Effect of Static Pressure on Intracellular pH of Adhesive Chinese Hamster Ovary Cells

Masashi Fujiwara,[1] Satoru Koizumi,[1] and Mutsumi Takagi[1]*

*Division of Biotechnology and Macromolecular Chemistry, Graduate School of Engineering, Hokkaido University, Kita 13, Nishi 8, Kita-ku, Sapporo 060-8628, Japan*[1]

Received 26 June 2007/Accepted 3 September 2007

**The effect of static pressure on the intracellular pH of the Chinese hamster ovary (CHO) cell line DR1000L4N was investigated. In cultivation of CHO cells at 0.9 MPa, two distinct populations were observed in the histogram of a flow cytometer, while single population was observed in cultivation at 0.1 MPa. The intracellular pH of the major population at 0.9 MPa was markedly lower than that of the single population at 0.1 MPa.**

[**Key words:** static pressure, intracellular pH, Chinese hamster ovary cells]

Recently, the importance of mammalian cell culture for the production of pharmaceutical substances has been increasing owing to the efficient use of such culture for the production of not only interferons (1) and tissue plasminogen activator (tPA) (2) but also antibodies. Static pressure is one of the operational parameters that is effective in increasing the supply rate of dissolved oxygen in mammalian cell culture. Although the effects of pH, temperature, dissolved oxygen concentration and agitation rate on mammalian cell culture have been well documented, there are only few reports on the effect of static pressure on mammalian cells as discussed below.

We have reported that pressurized cultivation at 0.9 MPa increases the specific production rate of monoclonal antibodies by mouse hybridoma cells (3), tPA by human embryo lung (HEL) cells (4) and human-granulocyte-macrophage colony stimulating factor (hGM-CSF) by Chinese hamster ovary (CHO) cells (5), although there is almost no influence of such pressurization on specific cell growth rate. We also suggested that the transduction of a static pressure signal for the enhanced expression of hGM-CSF mRNA in CHO cells is via an extracellular-signal-related kinase (ERK) signaling cascade (6).

On the other hand, high hydrostatic pressure (40–60 MPa) evidently decreases the vacuolar pH of cells of the yeast *Saccharomyces cerevisiae* (7). The acidification of yeast vacuoles is explained by the influx of protons into vacuoles from an acidified cytoplasm under high hydrostatic pressure (8, 9). It is possible that a similar cytoplasm acidification occurs in CHO cells when high hydrostatic pressure is applied to the cells. The resulting low intracellular pH may positively affect the activity of cytoplasmic enzymes involved in hGM-CSF production. However, there are few reports on the intracellular pH in mammalian cells under high pressure, despite the fact that CHO cells are one of most useful mammalian cells for pharmaceutical production. In this study, the effect of static pressure on the intracellular pH of CHO cells was investigated.

CHO DR1000L4N cells producing hGM-CSF (10) were cultivated in Iscove's modified Dulbecco's medium (Sigma, St. Louis, MO, USA) supplemented with 10% dialyzed fetal bovine serum (Gibco, Grand Island, NY, USA), 0.1 mg/ml streptomycin (Sigma), 100 U/ml penicillin (Sigma) and 1 μM methotrexate (Sigma).

The cells were inoculated into 5 ml of the medium in T-flasks (25 $cm^2$; Sumilon, Tokyo) at a density of $1.5 \times 10^4$ cells/$cm^2$ and incubated in a $CO_2$ incubator for 24 h (37°C and 5% $CO_2$). Then, the flasks were placed in a pressurized incubator system consisting of four stainless-steel vessels (120 mm in length and 95 mm in inner diameter) sealed using flanges fitted with valves, a pressure gauge, and a PVA filter (5). The gas in the vessels were replaced with a gas mixture of 5% $CO_2$ and 95% air. Two vessels were further pressurized to 0.9 MPa using nitrogen gas. Culture temperature was maintained at 37°C using a water bath, and the pressurized vessels were not opened until the end of cultivation. The partial pressures of $O_2$ and $CO_2$ in the T-flasks in the vessels were respectively set at 0.021 and 0.005 MPa independent of static pressure to prevent changes in pH and dissolved oxygen concentration at different pressures. The pH of the medium in a centrifuge tube placed in the pressurized vessel was measured immediately after opening the vessels to confirm that there is no difference in $CO_2$ gas partial pressure between the pressurized vessels at 0.1 and 0.9 MPa (data not shown).

The cell concentration in the culture was determined by nuclei staining, in which adhering cells were incubated in a solution of 21 g/*l* citrate and 1 g/*l* crystal violet, and nuclei were counted under a microscope (11). The hGM-CSF concentration in the culture supernatant was determined using an enzyme-linked immunosorbent assay kit (Pierce Endogen, Rockford, IL, USA).

A fluorescent reagent, 2′,7′-bis(2-carboxyethyl)-5(6)-car-

* Corresponding author. e-mail: takagi-m@eng.hokudai.ac.jp
phone/fax: +81-(0)11-706-6567

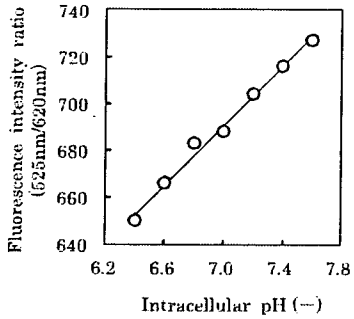


FIG. 1. Correlation between intracellular pH and fluorescence intensity ratio. CHO DR1000L4N cells were placed in high-[$K^+$] buffers (pHs 6.4, 6.6, 6.8, 7.0, 7.2, 7.4 and 7.6) for 5 min and incubated in EBSS buffer containing a fluorescent reagent, BCECF-AM, for 30 min. The fluorescence intensity of BCECF was measured at 525 nm and 620 nm using a flow cytometer. Internal pH was plotted against the mode of the ratio of the fluorescence intensity at 525 nm to that at 620 nm.

boxyfluorescein acetoxymethyl ester (BCECF-AM) (Sigma), was used for measuring the intracellular pH of CHO cells. The reagent permeates inside cells and is converted to the fluorescence dye BCECF through an intracellular esterase reaction, whose fluorescence intensity depends on intracellular pH. 5-(*N*-Ethyl-*N*-isopropyl) amiloride (EIPA, 100 μM) (Sigma) was added to cells in the late-logarithmic phase to maintain intracellular pH during BCECF-AM permeation. Then, the cells were harvested by trypsinization, washed once with EBSS buffer (sodium chloride, 140 mM; pottasium chloride, 5.4 mM; calcium chloride, 1.8 mM; magnesium sulfate, 0.8 mM; glucose, 5.0 mM, and HEPES 25 mM; pH 7.3±0.1), resuspended to a concentration of $1\times10^7$ cells/ml in EBSS buffer and incubated with 10 μM BCECF-AM for 30 min at room temperature. Fluorescence intensity was measured at 525 and 620 nm at an excitation of 488 nm using a flow cytometer (EPICS XL EXPO32 ADC; Beckman Coulter, Miami, FL, USA). CHO cells that were placed in high-[$K^+$] buffers (pHs 6.4, 6.6, 6.8, 7.0, 7.2, 7.4 and 7.6) containing 10 μM nigericin (Sigma) for 5 min, as mentioned above, were analyzed using a flow cytometer as controls and pH was plotted against the ratio of the intensity at 525 nm to that at 620 nm.

To precheck the accuracy of intracellular pH measurement, a calibration curve was plotted for CHO cells cultivated at 0.1 MPa. A good positive correlation was obtained between intracellular pH and fluorescence intensity ratio, as shown in Fig. 1.

After the adhesion of the CHO cells in the T-flask at 0.1 MPa for 24 h, the cells were cultured in the pressurized incubator at constant static pressures of 0.1 and 0.9 MPa. There was no marked difference between the cell densities on day 6 at 0.1 and 0.9 MPa (Table 1). Histograms of the

TABLE 1. Effect of static pressure on cell density of CHO cells at 143 h of cultivation

| Pressure (MPa) | Cell density ($10^5$ cells/cm$^2$) |
|---|---|
| 0.1 | 1.38±0.08 |
| 0.9 | 1.29±0.11 |

All results are expressed as means±SD (n=3).

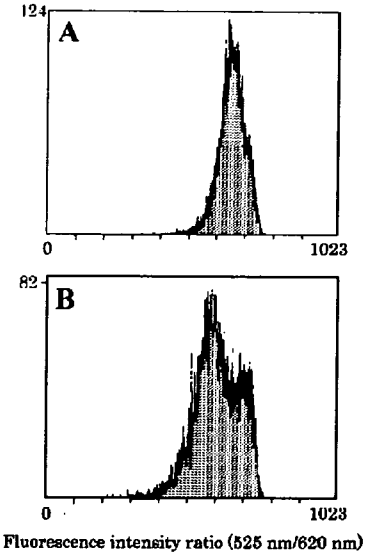


FIG. 2. Histogram of fluorescence intensity ratio. CHO DR1000L4N cells were cultured at constant pressures of 0.1 MPa (A) and 0.9 MPa (B) and incubated in EBSS buffer containing a fluorescent reagent, BCECF-AM, for 30 min. The fluorescence intensity of BCECF was measured at 525 nm and 620 nm using a flow cytometer. Total cell numbers in the histograms were 11391 (A) and 12948 (B), respectively.

fluorescence intensity ratio at 525 nm to that at 620 nm for the cells cultivated at 0.1 and 0.9 MPa are shown in Fig. 2. The histogram for the cells cultivated at 0.1 MPa showed a single peak whose ratio at 525 nm to that at 620 nm was approximately 650 (Fig. 2A). On the other hand, that for the cells cultivated at 0.9 MPa showed two distinct peaks. The ratio of mode for the larger peak (570) was lower than that for the cells cultivated at 0.1 MPa (650) (Fig. 2B). The smaller peak for the cells cultivated at 0.9 MPa had a higher ratio of mode (680) than that for the cells cultivated at 0.1 MPa (Fig. 2B).

The intracellular pHs at both 0.1 and 0.9 MPa of the CHO cells were calculated using the mode of the ratio in the histogram and calibration curve (Fig. 3). The intracellular pH for the larger peak of two populations in cultivation at 0.9 MPa (5.24±0.17) was markedly lower than that for the single peak at 0.1 MPa (6.60±0.76), and this difference (1.36) was considered significant at $P<0.05$ using a *t*-test. On the other hand, the intracellular pH for the smaller peak of the cells cultivated at 0.9 MPa was 6.77±0.09, which did not significantly differ from the intracellular pH of the cells cultivated at 0.1 MPa. Thus, it was found that increasing static pressure promotes cytoplasm acidification in major population of CHO cells.

Abe and Horikoshi have suggested that the following chemical reactions of $CO_2$, *i.e.*, hydration of carbon dioxide (Eq. 1) and ionization of carbonic acid (Eq. 2), contribute to cytoplasm acidification in yeast under high pressure (8, 9).

$$CO_2+H_2O \rightarrow H_2CO_3 \quad (1)$$

$$H_2CO_3 \rightarrow H^++HCO_3^- \quad (2)$$

$$CO_2+H_2O \rightarrow H^++HCO_3^- \quad (3)$$

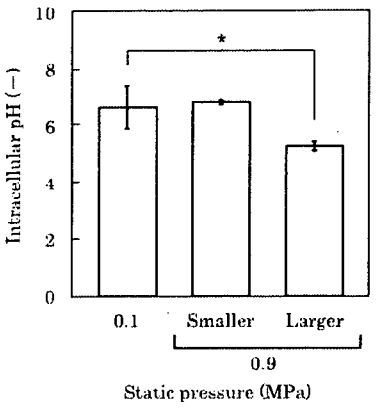


FIG. 3. Effect of static pressure on intracellular pH. CHO DR1000L4N cells were cultured at constant static pressures of 0.1 MPa and 0.9 MPa. The intracellular pH of CHO cells was determined from the mode of the ratio of the fluorescence intensities of BCECF measured by a flow cytometer. A single peak was observed at 0.1 MPa, and a larger peak and a smaller peak were observed at 0.9 MPa. The bar shows the SD of measurement (n=3) (asterisk: $P<0.05$).

The contribution of chemical reactions 1 and 2 to the reduction in the intracellular pH of CHO DR1000L4N cells was estimated as described below. The equilibrium equation in these two reactions can be represented by the equilibrium equation as follows (12):

$$\frac{\partial \ln k}{\partial P} = -\frac{\Delta V^{\#}}{RT} \tag{4}$$

where $P$ [atom] is the static pressure, $k$ is the rate constant, $\Delta V^{\#}$ is the volume of activation (=−26.0 ml/mol for Eq. 3), $R$ is the gas constant (=8.31 J/K mol), and $T$ is the absolute temperature (=310 K).

By substituting these values into Eq. 4, $\partial \ln k/\partial P$ can be calculated using

$$\frac{\partial \ln k}{\partial P} = -\frac{(-26.0)}{8.31 \times 310} = 1.01 \times 10^{-2} \tag{5}$$

When $k_1$ and $k_2$ are incorporated into Eq. 5 as rate constants at 0.1 MPa ($P_1$) and 0.9 MPa ($P_2$), respectively, Eq. 5 can be converted to

$$[\ln k]_{k_1}^{k_2} = 1.01 \times 10^{-2} [P]_{P_1}^{P_2} \tag{6}$$

$$\frac{k_2}{k_1} = \exp(8.08 \times 10^{-2}) = 1.08 \tag{7}$$

Equation 7 shows that the rate constant at 0.9 MPa ($k_2$) was 1.08 times larger than that at 0.1 MPa ($k_1$). Therefore, the difference between the pHs at 0.1 and 0.9 MPa (ΔpH) can be calculated based on the equilibrium of chemical reaction 2 as follows:

$$\Delta pH = \left(-\log k + \log \frac{[HCO_3^-]}{[H_2CO_3]}\right) - \left(-\log(1.08k) + \log \frac{[HCO_3^-]}{[H_2CO_3]}\right) = 0.033 \tag{8}$$

The calculated ΔpH (0.033) was considerably smaller than the experimentally observed ΔpH (1.36) in Fig. 3. This suggests that another mechanism, such as (i) proton generation from glycolytic intermediates and inorganic phosphates, and (ii) inactivation of the plasma membrane $H^+$-ATPase (8, 9), rather than the hydration and ionization of carbon dioxide, contribute to the decrease in the intracellular pH of pressurized CHO cells. Such other contributions should be investigated in the future.

There should be few report about the intracellular pH of mammalian cell culture under high pressure. In this study, we first quantitatively estimated the intracellular pH change in cultivation of CHO cells under high pressure by using a fluorescent reagent and a flow cytometer. It was found that the intracellular pH of major population of CHO DR1000L4N was obviously decreased when high pressure was applied to the cells.

## REFERENCES

1. **Kawade, Y.:** Induction of antiviral resistance and interferon production in animal cell culture by exogenous RNA. Jpn. J. Med. Sci. Biol., **24**, 130–131 (1971).
2. **Dater, R. V., Cartwright, T., and Rosen, C. G.:** Process economics of animal cell and bacterial fermentations: a case study analysis of tissue plasminogen activator. Biotechnology, **11**, 349–357 (1993).
3. **Takagi, M., Ohara, K., and Yoshida, T.:** Effect of hydrostatic pressure on hybridoma cell metabolism. J. Ferment. Bioeng., **80**, 619–621 (1995).
4. **Takagi, M., Okumura, H., Okada, T., Kobayashi, N., Kiyota, T., and Ueda, K.:** An oxygen supply strategy for the large-scale production of tissue plasminogen activator by microcarrier cell culture. J. Ferment. Bioeng., **77**, 301–306 (1994).
5. **Gong, H., Takagi, M., Moriyama, T., Ohno, T., and Yoshida, T.:** Effect of static pressure on human granulocyte-macrophage stimulating factor (hGM-CSF) production by Chinese hamster ovary cells. J. Biosci. Bioeng., **94**, 271–274 (2002).
6. **Gong, M., Takagi, M., and Yoshida, T.:** Transduction of static pressure signal to expression of human granulocyte macrophage colony stimulating factor mRNA in Chinese hamster ovary cells. J. Biosci. Bioeng., **96**, 79–82 (2003).
7. **Abe, F. and Horikoshi, K.:** Hydrostatic pressure promotes the acidification of vacuoles in *Saccharomyces cerevisiae*. FEMS Microbiol. Lett., **130**, 307–312 (1995).
8. **Abe, F. and Horikoshi, K.:** Vacuolar acidification in *Saccharomyces cerevisiae* induced by elevated hydrostatic pressure is transient and is mediated by vacuolar $H^+$-ATPase. Extremophiles, **1**, 89–93 (1997).
9. **Abe, F. and Horikoshi, K.:** Analysis of intracellular pH in the yeast *Saccharomyces cerevisiae* under elevated hydrostatic pressure: a study in baro-(piezo-)physiology. Extremophiles, **2**, 223–228 (1998).
10. **Yoshikawa, T., Nakanishi, F., Ogura, Y., Oi, D., Omasa, T., Katakura, Y., Kishimoto, M., and Suga, K.:** Amplified gene location in chromosomal DNA affected recombinant protein production and stability of amplified genes. Biotechnol. Prog., **16**, 710–715 (2000).
11. **Sanford, K. K., Earle, W. R., Evans, V. J., Walts, H. K., and Shannon, J. E.:** The measurement of proliferation in tissue cultures by enumeration of cell nuclei. J. Natl. Cancer Inst., **11**, 773–795 (1951).
12. **Morild, E.:** The theory of pressure effect on enzymes. Adv. Protein Chem., **34**, 93–166 (1981).

Journal of Cerebral Blood Flow & Metabolism (2008), 1–4
 0271-678X/08 $30.00
www.jcbfm.com

## Brief Communication

# Increase in circulating CD34-positive cells in patients with angiographic evidence of moyamoya-like vessels

Tomoyuki Yoshihara[1], Akihiko Taguchi[1], Tomohiro Matsuyama[2], Yoko Shimizu[1], Akie Kikuchi-Taura[3], Toshihiro Soma[3], David M Stern[4], Hiroo Yoshikawa[5], Yukiko Kasahara[1], Hiroshi Moriwaki[1], Kazuyuki Nagatsuka[1] and Hiroaki Naritomi[1]

[1]*Department of Cerebrovascular Disease, National Cardiovascular Center, Osaka, Japan;* [2]*Institute for Advanced Medical Sciences, Hyogo College of Medicine, Hyogo, Japan;* [3]*Department of Hematology, Osaka Minami National Medical Center, Osaka, Japan;* [4]*Dean's Office, College of Medicine, University of Cincinnati, Cincinnati, Ohio, USA;* [5]*Department of Internal Medicine, Hyogo College of Medicine, Hyogo, Japan*

**Increasing evidence points to a role for circulating endothelial progenitor cells, including populations of CD34-positive (CD34$^+$) cells, in maintenance of cerebral blood flow. In this study, we investigated the link between the level of circulating CD34$^+$ cells and neovascularization at ischemic brain. Compared with control subjects, a remarkable increase of circulating CD34$^+$ cells was observed in patients with angiographic moyamoya vessels, although no significant change was observed in patients with major cerebral artery occlusion (or severe stenosis) but without moyamoya vessels. Our results suggest that the increased level of CD34$^+$ cells associated with ischemic stress is correlated with neovascularization at human ischemic brain.**
*Journal of Cerebral Blood Flow & Metabolism* advance online publication, 30 January 2008; doi:10.1038/jcbfm.2008.1

**Keywords:** antigens; CD34; moyamoya vessel; neovascularization

## Introduction

Increasing evidence points to a role for bone marrow-derived immature cells, such as endothelial progenitor cells, in maintenance of vascular homeostasis and repair. CD34-positive (CD34$^+$) cells comprise a population enriched for endothelial progenitor cells whose contribution to neovasculature includes both direct participation in forming the neovessel and regulatory roles as sources of growth/angiogenesis factors (Majka *et al*, 2001). Previously, we have shown accelerated neovascularization after administration of CD34$^+$ cells in an experimental model of stroke (Taguchi *et al*, 2004*b*) and induced by autologous bone marrow mononuclear cells (rich cell fraction of CD34$^+$ cells) transplanted locally into patients with limb ischemia (Taguchi *et al*, 2003). In addition, we have observed a positive correlation between the level of circulating CD34$^+$ cells and regional blood flow (Taguchi *et al*, 2004*a*), and cognitive function (Taguchi *et al*, 2007) in patients with chronic cerebral ischemia.

In this study, we have evaluated the level of circulating CD34$^+$ cells in patients with unusually accelerated neovascularization induced by progressive occlusion (or severe stenosis) of the supraclinoid portion of the internal carotid artery, the proximal region of the anterior, and/or middle cerebral artery characterized angiographically by the presence of moyamoya-like vessels (Natori *et al*, 1997) that supply ischemic brain as collaterals. We have investigated the hypothesis that circulating bone marrow-derived immature cells might be associated with neovascularization at ischemic sites in the human brain.

## Patients and methods

The institutional review board of the National Cardiovascular Center approved this study. All subjects provided

Correspondence: Dr A Taguchi, Department of Cerebrovascular Disease, National Cardiovascular Center, 5-7-1 Fujishiro-dai, Suita, Osaka 565-8565, Japan.
E-mail: taguchi@ri.ncvc.go.jp
This work was supported by a Grant-in-Aid for Scientific Research from the Ministry of Health, Labour, and Welfare (H19-Choujyu-029).
Received 29 October 2007; revised 19 December 2007; accepted 26 December 2007

informed consent. A total of 50 individuals, including 24 patients with occlusion or severe stenosis (>90%) at the C1 portion of the internal carotid artery or the M1 portion of the middle cerebral artery, and 26 age-matched healthy volunteers with cardiovascular risk factors, but without history of vascular disease, were enrolled. The diagnosis of cerebral artery occlusion or stenosis was made angiographically and four patients were found to have classical angiographic evidence of moyamoya-like vessels, including one with right C1 occlusion, one with right M1 occlusion, and two with bilateral C1 severe stenosis. All patients with cerebral artery occlusion or stenosis had a history of cerebral infarction. Individuals excluded from the study included patients who experienced a vascular event within 30 days of measurements, premenopausal women, and those with evidence of infection and/or malignant disease. The number of circulating $CD34^+$ cells was quantified as described (Taguchi *et al*, 2007). In brief, blood samples (200 $\mu$l) were incubated with phycoerythrin-labeled anti-CD34 antibody, fluorescein isothiocyanate-labeled anti-CD45 antibody, 7-aminoactinomycin-D (7-AAD), and internal control (all of these reagents are in the Stem-Kit; BeckmanCoulter, Marseille, France). After incubation, samples were centrifuged, and supernatant was removed to obtain concentrated cell suspensions. 7-Aminoactinomycin-D-positive dead cells and CD45-negative cells were excluded, and the number of cells forming clusters characteristic of $CD34^+$ cells (i.e., low side scatter and low-to-intermediate CD45 staining) was counted. The absolute number of $CD34^+$ cells was calculated using the internal control. Mean cell number of duplicate measurements was used for quantitative analysis. Statistical comparisons among groups were determined using analysis of variance or $\chi^2$ test. Individual comparisons were performed using a two-tailed unpaired Students' *t*-test or Mann–Whitney's *U*-test. Mean ± s.e. is shown.

## Results

Enrolled individuals were divided into three groups: control subjects, patients with cerebral occlusion or severe stenosis, but without the presence of vessels with angiographic characteristics of moyamoya disease, and patients with angiographic evidence of moyamoya-like vessels. Baseline characteristics of the groups are shown in Table 1. The modified Rankin scale evaluation of patients with and without moyamoya-like vessels was $0.5 \pm 0.5$ and $1.3 \pm 0.2$, respectively ($P = 0.15$). Comparing these groups, there was a significant difference in the ratio of gender and treatment with aspirin between groups. However, no significant difference was observed in the number of circulating $CD34^+$ cells in control group between genders (male, $n = 13$, $CD34^+$ cells $= 0.93 \pm 0.10/\mu$L; female, $n = 13$, $CD34^+$ cells $= 0.85 \pm 0.11/\mu$L: $P = 0.59$) and treatment with aspirin (aspirin (+), $n = 6$, $CD34^+$ cells $= 0.76 \pm 0.12/\mu$L; aspirin (−), $n = 20$, $CD34^+$ cells $= 0.93 \pm 0.09/\mu$L: $P = 0.26$), indicating mild and nonsignificant effects of gender and treatment with aspirin on the level of circulating $CD34^+$ cells. In univariate analysis of control subjects, each cerebrovascular risk factor and treatment with statins showed no significant difference in the number of circulating $CD34^+$ cells (data not shown).

A representative angiogram showing characteristics of moyamoya-like vessels is shown in Figures 1A and 1B. Angiographic moyamoya-like vessels were observed around the M1 portion of an occluded middle cerebral artery. Compared with a normal subject (Figure 1C) and patients without angiographic evidence of moyamoya-like vessels (Figure 1D), a remarkable increase in levels of

**Table 1** Baseline characteristics

| | *Total* | *Control* | *Major artery occlusion/stenosis* | | *P-value for trend* |
|---|---|---|---|---|---|
| | | | *Moyamoya (−)* | *Moyamoya (+)* | |
| *N* | 50 | 26 | 20 | 4 | |
| Age, years | 60.8 ± 1.1 | 60.5 ± 1.9 | 61.5 ± 1.0 | 59.3 ± 5.9 | 0.85 |
| Male, *n* (%) | 33 (66) | 13 (50) | 18 (90) | 2 (50) | 0.01 |
| *Risk factor, n (%)* | | | | | |
| Hypertension | 35 (70) | 16 (62) | 15 (75) | 4 (100) | 0.24 |
| Hyperlipidemia | 26 (52) | 14 (54) | 10 (50) | 2 (50) | 0.96 |
| Diabetes mellitus | 11 (22) | 7 (27) | 4 (20) | 0 (0) | 0.46 |
| Smoking | 15 (30) | 7 (27) | 8 (40) | 0 (0) | 0.25 |
| *Treatment, n (%)* | | | | | |
| Ca channel blockers | 20 (40) | 10 (38) | 8 (40) | 2 (50) | 0.91 |
| β-Blockers | 5 (10) | 3 (11) | 1 (5) | 1 (25) | 0.44 |
| ACE inhibitor | 7 (14) | 4 (15) | 2 (10) | 1 (25) | 0.70 |
| ARB | 12 (24) | 5 (19) | 5 (25) | 2 (50) | 0.40 |
| Diuretics | 4 (8) | 2 (7) | 1 (5) | 1 (25) | 0.40 |
| Statin therapy | 14 (28) | 9 (34) | 4 (20) | 1 (25) | 0.54 |
| Aspirin | 19 (38) | 6 (23) | 10 (50) | 3 (75) | 0.05 |
| Ticlopidine | 12 (24) | 3 (11) | 8 (40) | 1 (25) | 0.08 |

Abbreviations: ACE, angiotensin-converting enzyme; ARB, angiotensin 2 receptor blocker.

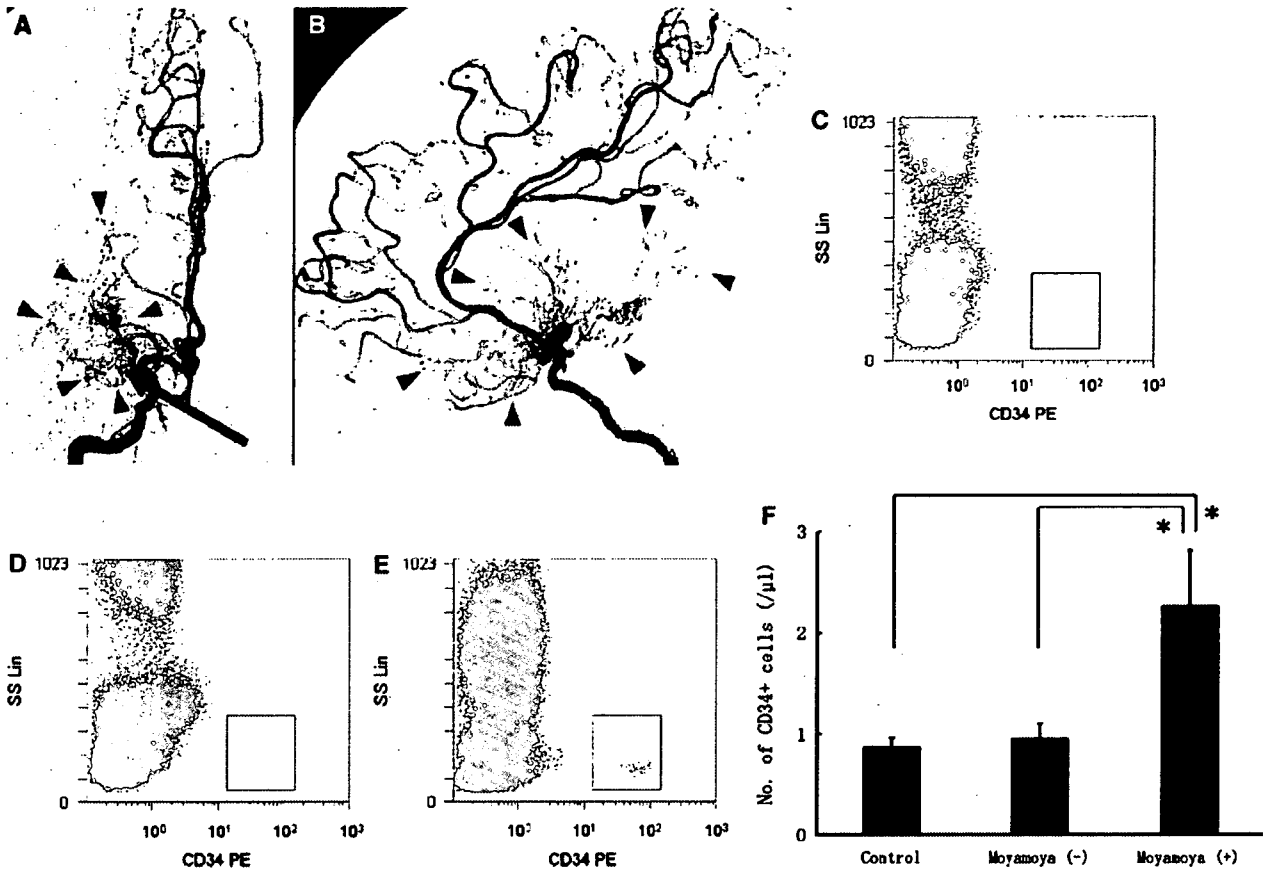


**Figure 1** Increased levels of circulating CD34+ cells in patients with angiographic evidence of moyamoya-like vessels. (**A, B**) Representative angiogram from a patient with moyamoya-like vessels. Unusually accelerated neovascularization (based on angiographic features of moyamoya-like vessels, arrowheads) was observed around an occlusive M1 lesion (arrow). Anterior–posterior view (**A**) and lateral view (**B**) of the right internal carotid artery showed angiographically. (**C–E**) After exclusion of 7-aminoactinomycin-D (7-AAD)-positive dead cells and CD45-negative cells (nonleukocytes), CD34+ cells cluster at low side scatter. Representative fluorescence-activated cell sorting analyses from a control subject (**C**), a patient without moyamoya-like vessels (**D**), and a patient with moyamoya-like vessels (**E**) are shown. (**F**) A more than two-fold increase in circulating CD34+ cells was observed in patients with moyamoya-like vessels, compared with control subjects and patients without moyamoya-like vessels (*$P < 0.001$). SS Lin: side-scatter linear scale.

peripheral CD34+ cells was observed in patients with moyamoya-like vessels (Figure 1E) based on fluorescence-activated cell sorting. To confirm this impression, levels of circulating CD34+ cells were quantified (control, CD34+ cells = $0.89 \pm 0.07/\mu L$; moyamoya (−), CD34+ cells = $0.98 \pm 0.13/\mu L$; moyamoya (+), CD34+ cells = $2.28 \pm 0.53/\mu L$) and found to be significantly increased in patients with moyamoya-like vessels more than two-fold higher than in controls (Figure 1F, $P < 0.001$).

## Discussion

In this study, we have found that a feature of unusually accelerated neovascularization, evidence of moyamoya-like vessels in the immediate locale of an occluded major cerebral artery, can be correlated with a robust increase in the level of circulating CD34+ cells. The latter was determined using a newly developed method that enables quantification of few CD34+ cells in peripheral blood in a highly reproducible manner.

After acute cerebral ischemia, mobilization of CD34+ cells from bone marrow has been shown in stroke patients (Taguchi *et al*, 2004*a*). Furthermore, transplantation of CD34+ cells (Taguchi *et al*, 2004*b*) and bone marrow cells (Borlongan *et al*, 2004*a*, *b*) has been shown to restore cerebral blood flow in experimental models of stroke. In chronic ischemia, transplantation of CD34+ cells has also been shown to accelerate neovascularization, including formation of collateral vessels, in patients with chronic ischemic heart disease (Boyle *et al*, 2006) and limb ischemia (Kudo *et al*, 2003). In addition, there is a report regarding the correlation between inadequate coronary collateral development and reduced numbers of circulating endothelial progenitor cells in

patients with myocardial ischemia (Lambiase *et al*, 2004). In this study, we show, for the first time, a correlation between neovascularization of the cerebral arterial circulation and increased levels of circulating CD34+ cells. Our results support the hypothesis that circulating CD34+ cells potentially contribute to neovascularization at sites of ischemic brain injury.

## Acknowledgements

We thank K Obata and Y Okinaka for technical assistance.

## Conflict of interest

The authors state no conflict of interest.

## References

Borlongan CV, Lind JG, Dillon-Carter O, Yu G, Hadman M, Cheng C, Carroll J, Hess DC (2004*a*) Bone marrow grafts restore cerebral blood flow and blood brain barrier in stroke rats. *Brain Res* 1010:108–16

Borlongan CV, Lind JG, Dillon-Carter O, Yu G, Hadman M, Cheng C, Carroll J, Hess DC (2004*b*) Intracerebral xenografts of mouse bone marrow cells in adult rats facilitate restoration of cerebral blood flow and blood–brain barrier. *Brain Res* 1009:26–33

Boyle AJ, Whitbourn R, Schlicht S, Krum H, Kocher A, Nandurkar H, Bergmann S, Daniell M, O'Day J, Skerrett D, Haylock D, Gilbert RE, Itescu S (2006) Intra-coronary high-dose CD34+ stem cells in patients with chronic ischemic heart disease: a 12-month follow-up. *Int J Cardiol* 109:21–7

Kudo FA, Nishibe T, Nishibe M, Yasuda K (2003) Autologous transplantation of peripheral blood endothelial progenitor cells (CD34+) for therapeutic angiogenesis in patients with critical limb ischemia. *Int Angiol* 22:344–8

Lambiase PD, Edwards RJ, Anthopoulos P, Rahman S, Meng YG, Bucknall CA, Redwood SR, Pearson JD, Marber MS (2004) Circulating humoral factors and endothelial progenitor cells in patients with differing coronary collateral support. *Circulation* 109:2986–92

Majka M, Janowska-Wieczorek A, Ratajczak J, Ehrenman K, Pietrzkowski Z, Kowalska MA, Gewirtz AM, Emerson SG, Ratajczak MZ (2001) Numerous growth factors, cytokines, and chemokines are secreted by human CD34(+) cells, myeloblasts, erythroblasts, and megakaryoblasts and regulate normal hematopoiesis in an autocrine/paracrine manner. *Blood* 97:3075–85

Natori Y, Ikezaki K, Matsushima T, Fukui M (1997) 'Angiographic moyamoya' its definition, classification, and therapy. *Clin Neurol Neurosurg* 99(Suppl 2): S168–72

Taguchi A, Matsuyama T, Moriwaki H, Hayashi T, Hayashida K, Nagatsuka K, Todo K, Mori K, Stern DM, Soma T, Naritomi H (2004*a*) Circulating CD34-positive cells provide an index of cerebrovascular function. *Circulation* 109:2972–5

Taguchi A, Matsuyama T, Nakagomi T, Shimizu Y, Fukunaga R, Tatsumi Y, Yoshikawa H, Kikuchi-Taura A, Soma T, Moriwaki H, Nagatsuka K, Stern DM, Naritomi H (2007) Circulating CD34-positive cells provide a marker of vascular risk associated with cognitive impairment. *J Cereb Blood Flow Metab*; e-pub ahead of print 8 August 2007

Taguchi A, Ohtani M, Soma T, Watanabe M, Kinosita N (2003) Therapeutic angiogenesis by autologous bone-marrow transplantation in a general hospital setting. *Eur J Vasc Endovasc Surg* 25:276–8

Taguchi A, Soma T, Tanaka H, Kanda T, Nishimura H, Yoshikawa H, Tsukamoto Y, Iso H, Fujimori Y, Stern DM, Naritomi H, Matsuyama T (2004*b*) Administration of CD34+ cells after stroke enhances neurogenesis via angiogenesis in a mouse model. *J Clin Invest* 114:330–8

Available online at www.sciencedirect.com
ScienceDirect
Behavioural Brain Research 179 (2007) 90–98
BEHAVIOURAL BRAIN RESEARCH
www.elsevier.com/locate/bbr

Research report

# Environmental change during postnatal development alters behaviour, cognitions and neurogenesis of mice

Hiroyuki Iso [a,*], Shigero Simoda [a], Tomohiro Matsuyama [b]

[a] *Department of Behaviour Science, Hyogo College of Medicine, 1-1 Mukogawa-cho, Nishinomiya, Hyogo 663-8501, Japan*
[b] *Institute for Advanced Medical Sciences, Hyogo College of Medicine, 1-1 Mukogawa-cho, Nishinomiya, Hyogo 663-8501, Japan*

Received 22 March 2006; received in revised form 4 January 2007; accepted 23 January 2007
Available online 3 February 2007

**Abstract**

Four groups of male C57BL/6 mice were reared differing combinations of the two environments from 3 to 11 weeks after birth. At 12 and 13 weeks they were assessed by measures of behaviour and learning: open-field activity, auditory startle reflex and prepulse inhibition, water maze learning, and passive avoidance. Another four groups of mice reared under these varying conditions were examined for generation of neurons in hippocampus and cerebral cortex using bromodeoxyuridine (BrdU) at 12 weeks. Enriched (EE) and impoverished (PP) groups were housed in their respective environment for 8 weeks, enriched–impoverished (EP) and impoverished–enriched (PE) mice respectively were reared for 6 weeks in the first-mentioned environment and then for 2 weeks in the second. PP and EP mice showed hyperactivity, greater startle amplitude and significantly slower learning in a water maze than EE or PE animals, and also showed a memory deficit in a probe test, avoidance performance did not differ. Neural generation was greater in the EE and PE than PP and EP groups, especially in the hippocampus. These results suggest that environmental change critically affects behavioural and anatomic brain development, even if brief. In these mice, the effect of unfavourable early experience could be reversed by a later short of favourable experience.


*Keywords:* Enrichment; Impoverishment; Environmental change; Behaviour; Neuronal generation; Mice

## 1. Introduction

Research concerning environmental enrichment has been carried out since 1960s. Earlier studies reported that rats reared for a few months following weaning in a group in a large cage with a running wheel, toys and a hiding had greater brain weights and showed more acetylcholinesterase activity than animals reared alone in a small cage for the same period even though both environments had food and water continuously available [38,40]. Some authors suspected that an increase in glial cells might have contributed to these differences [2]. Later, rats spending earlier life in an enriched environment had been reported to show lower activity in open field test than rats spending the same period in an impoverished setting with little stimulation [17]. Still other reports indicated that even brief exposure to the enriched environment affected development of brain and behaviour in rats [11,12]. In recent studies involving rats, an enriched developmental environment was reported to increase neurotrophic factor gene expression [29], brain-derived neurotrophic factor protein [30], numbers of hippocampal neurons [20,21,48,49], and dendritic growth, in association with improvements in behaviour and cognition [22]. Recovery from transient global ischemia was reported clinically to be promoted by environment enrichment [15]. Environmental enrichment also was reported to promote normal emotional behaviour and even immune function under stress [5]. Even "knockout" mice with a genetically mediated hippocampal deficit causing behavioural and memory deficiencies were reported to improve their ability to learn after a period of exposure to an enriched environment [8,35]. Thus, a benefit from environmental enrichment during development of animals concerning behaviour, neurophysiology, neuroanatomy, and even immunity has been reported and even applied to humans [16,36,37].

On the other hand, some authors point out that an enriched environment is the natural situation in animal neurologic development, while environmental impoverishment is an artificial

*Abbreviations:* BrdU, 5-bromo-2′-deoxyuridine; PSA-NCAM, polysialylated neuronal cell adhesion molecule

* Corresponding author. Tel.: +81 798456378; fax: +81 798456378.
*E-mail address:* iso@hyo-med.ac.jp (H. Iso).

0166-4328/$ – see front matter © 2007 Elsevier B.V. All rights reserved.
doi:10.1016/j.bbr.2007.01.025

condition inducing neurologic maldevelopment [27,41]. Indeed, rats housed singly can show abnormal behaviours, such as attention deficiency, hyperactivity, exaggerated emotional behaviour, and stereotypy [6,51], accompanied by evidence of neurochemical change [24,31,32]. Lack of manipulation during infancy also was reported to impair learning and memory in the adult rat [34]. Socially isolated animals even have been studied as a model of human psychotic illness [6]. Some animal studies also have examined whether or not resocialization could reverse effects of social isolation. Hyperactivity and hypoanalgesia [14] as well as deficient in water-maze learning [50] in impoverished rats has been demonstrated to be reversible upon resocialization. However, other studies where impoverishment started at weaning period failed to show this effect [9,13], suggest that the developing brain is susceptible to permanent changes at an earlier age. Wright et al. [51] reported that rats reared in an impoverished environment for 30 days after weaning, could not reverse their profile of anxious behaviour in X-maze performance after resocialization for 30 days. The performance of rats experiencing the reverse condition (a change from enriched to impoverished environments) did not differ from that in the enrichment group. Thus, reversal of environmental conditions 30 days after weaning did not affect the animals' emotional profiles. Katz and Davies [19] tested the effects of environmental manipulation during developing period on the neuroanatomy of the rats using a factorial design. Two groups of animals were reared in the enriched or impoverished environment for 2 months. Another two groups of rats were housed enriched or impoverished environment for 1 month, then the housing condition was changed to impoverished or enriched in the next month, respectively. The neuroanatomical outcomes of the enriched and impoverished groups supported to earlier reports by Rosenzweig et al. [38,40] that enriched rats had heavier brain weight, longer cerebral length and greater cortical thickness than impoverished rats. The results of the two exchange groups showed that animals which experienced enriched housing whichever during early or later 1 month developed their brain as same as the enriched group. Thus, enrichment was beneficial for brain development, and development of the brain was not modified by impoverishment, once rats had experienced enrichment [19].

The finding of neurogenesis in the adult rat [43,44] involves methods for discriminating newly generated neurons from established cell masses in the various areas of the brain. Much evidence has accumulated about effects of environment on brain development [2,21–23,29,30,38]. Additionally, experience with running was reported to enhance neurogenesis and promoted long-term potentiation (LTP) and learning in mice [47,48]. Yet, little has been known about effects of environmental manipulation during development on generation of neurons in adult rodents [20,21,48,49].

Whether enrichment or impoverishment is a more important environmental influence on neural development, neuronal plasticity suggests that exposure of impoverished animals to an enriched environment will enhance behavioural performance, while the reverse sequence will impair performance even if it is a short duration [11,12]. The objects of the present experiment are to test whether the environmental manipulations, from enrichment to impoverishment, or impoverishment to enrichment affect to the behavioural and neuronal development in mice [19], because we have experienced behavioural and neuroanatomical experiments in mice [25,52,53,1,45] and mice were drawn attention as models of human behavioural and psychiatric diseases rather than rats due to the developing evidences by gene engineering [7].

## 2. Materials and methods

All procedures were performed in accordance with National Cardiovascular Center Animal Care and Use Protocol. Quantitative measurements including behavioural tests and microscopic assessments were performed by investigators without knowing identity of the animal or section under study.

### 2.1. Experiment 1: behaviour

The effect of environmental manipulations on activity, reflexes, attention and cognition, spatial learning and of memory of fear were examined.

#### 2.1.1. Subjects

Forty-four male C57BL/6 mice, purchased from Nihon SLC (Shizuoka Japan) of age at 3 weeks were reared under four different housing conditions for 8 weeks. Tap water and food (MF chow, Oriental, Tokyo Japan) were continuously available. In the enriched (EE) group, mice were housed for 8 weeks four animals to a plastic cage (60 cm × 80 cm × 30 cm) containing plastic tubes as toys, a hiding place, and a running wheel. Mice in the impoverished (PP) group were housed for 8 weeks singly in a small plastic cage (20 cm × 30 cm × 20 cm) with no play materials. Enriched–impoverished (EP) mice first were housed like EE mice for 6 weeks and then like PP mice for 2 weeks. Impoverished–enriched (PE) mice were housed like PP mice for 6 weeks and then like EE mice for 2 weeks. Mice were handled once weekly for less than 1 min to weigh them and place them in clean cages. The two connected rooms where mice were housed and tested were air conditioned to maintain temperatures between 20 and 21 °C. Room lights were on from 7 a.m. to 7 p.m.

### 2.2. Apparatus and experimental protocol

Behavioural tests (one to four below) were conducted in order of description (and of increasing complexity) to avoid order effects [26]. The basic experimental settings of the open-field test, Morris water maze learning and passive avoidance task were reported previously [25,52]. All the behavioural tests were conducted during light period (10:00–16:00 h), and the group order of animals applied to each test was random. Mixed-type analyses of variance (ANOVA) were used for data analysis. Differences between groups were tested further with a post hoc test (Bonferroni/Dunn, with $p < .05$ defining significance).

#### 2.2.1. Open-field test

Animals were allowed to move freely in a square acrylic box (30 cm × 30 cm) for 20 min. Ten minutes light period was followed by 10-min dark period. On X and Y sides of the open-field, two infrared beams were positioned 2 cm above the box floor at a 10-cm distance. A flip-flop circuit was set up between the two beams. The total number of beam crossings was counted as locomotive behaviour of the animal. On the X side, 12 other infrared beams were positioned 5 cm above the floor at 3-cm intervals, and the total number of beam crossings was counted as rearing behaviour. After the session, stools left on the floor were counted.

#### 2.2.2. Acoustic startle reflex and prepulse inhibition test

Basic experimental settings were reported previously [42,53], we modified these for the present study. Briefly, the mouse was placed in a translucent acrylic cage (7 cm × 7 cm × 16.5 cm). Movements of the animal were detected by a piezoelectric accelerometer (GH313A, GA245SO; Keyence, Kyoto, Japan) attached at the bottom of cage. White noise at 115 dB (c) with duration of 50 ms was used as the acoustic startle stimulus (pulse). A noise prepulse of 85 dB (c)

was presented for 30 ms. Background noise was kept at a relatively constant level, 70–73 dB (c). The test session consisted of a total of 64 trials: 40 startle trials (habituation) without a prepulse, followed by 24 trials of prepulse test session. The mean inter-trial interval was 25 s (range, 15–45 s). In the prepulse trials prepulse with lead times of 50, 100, or 200 ms was followed by the pulse. In the prepulse test session, 12 pulse-alone trials and 12 prepulse trials were presented in random order. Relative startle response (RSR) was calculated using the formula RSR = PP/*N*, where PP designated the mean response with a prepulse, and *N* designated the mean response without a prepulse.

*2.2.3. Water maze learning*

A swimming tank 96 cm in diameter was used. Nontoxic India ink was added to the water to render it opaque. Water temperature was maintained at 20–24 °C. A platform 10 cm in diameter was positioned at a consistent point in the tank, submerged 5 mm below the surface of the water. In the learning trial, a mouse was placed in one of the three quadrants of the pool without platform. The experimenter determined the swimming time until reaching the platform (latency) using a stopwatch. When the animal reached the platform it was allowed to stay there for 10 s, and then was returned to a waiting box. If a mouse could not reach the platform within 60 s, the mouse was placed on the platform by the experimenter, and the latency was taken to be 60 s. The interval between trials was 30 s.

*2.2.4. Passive avoidance learning*

The apparatus consisted of two compartments, one lit and one dark, separated by a vertically sliding door. Mice initially were placed in the lit compartment. After the door was opened and the animal entered the dark compartment, the door was closed. After 10 s, a 3-s, 0.6-mA shock was delivered. The mouse was allowed to recover for 10 s and then returned to the home cage. Twenty-four hours later the mouse again was placed in the lit section with the door positioned opened to allow movement into the dark section. Latencies for stepping through the door were recorded.

*2.2.5. Assessment of brain weight*

After all behavioural tests, mice were killed by cervical dislocation. The brain was removed including the olfactory bulbs, the brainstem was cut at the level of the foramen magnum. Brain weighted at exactly 3 min after cervical dislocation.

*2.3. Experiment 2: neuroanatomy*

The effect of environmental manipulations on generation of neurons was examined using new mice.

*2.3.1. Subjects*

Twenty-eight male C57BL/6 mice, purchased from Nihon SLC (Shizuoka, Japan) when 3 weeks old, were reared for 8 weeks in four groups (each $n = 7$) with different housing conditions in the same manner as Experiment 1. Tap water and food (MF chow, Oriental, Tokyo, Japan) were continuously available.

*2.4. Experimental protocol*

*2.4.1. Cell proliferation analysis*

For assessment of cell proliferation *in vivo*, 5-bromo-2′-deoxyuridine (BrdU 200 mg/kg, Sigma–Aldrich) was administered intraperitoneally when mice reached to 12 weeks of age. After 24 h the four groups of mice were anaesthetized deeply with pentobarbital sodium (50 mg/kg) and fixed by transcardial perfusion with 4% paraformaldehyde. Then the brain was removed and postfixed for 24 h by immersion in 4% paraformaldehyde. Eight coronal slices 1 mm in thickness were made from the fixed forebrain using a rodent brain slicer (Acrylic Matrices, Alto, USA). Serial sections 20 μm in thickness were prepared from each slice with a vibratome (Leica, Wetzlar, Germany). Sections were subjected to double-labeling fluorescence immunohistochemistry with antibody to polysialylated neuronal cell adhesion molecule (PSA-NCAM, Chemicon International) as a marker of migrating neuronal progenitor cells (NPCs), and an antibody to BrdU (Boehringer Ingelheim, Mannheim, Germany).

Cells staining for both BrdU and PSA-NCAM according to confocal microscopy (Olympus, Tokyo Japan) were counted per high-power field (40× objective lens) as newly generated/proliferating neurons. For quantitative analysis, sections including the dentate gyrus of the hippocampus were stained, and BrdU/PSA-NCAM-positive cells in this granule cell layer were counted by two investigators blinded to the experimental protocol. The cell counted then was expressed as cells per millimetre of dentate gyrus. Cells in cerebral cortex stained for both BrdU and PSA-NCAM were counted in 10 fields of cingulate cortex, and the number of positive neocortical cells was expressed as cells per square millimetre.

## 3. Results

*3.1. Behavioural data*

*3.1.1. Body weight change*

Fig. 1 shows body weight change in the four groups of mice during the 8-week housing period. Mixed-type ANOVA indicated no significant main effect of group (G) [$F(3, 40) = 1.486$], while main effect of week (W) and interaction between G and W were significant [$F(7, 280) = 658.43$, $p < .0001$ and $F(21, 280) = 4.746$, $p < .0001$, respectively].

*3.1.2. Open-field activity*

Fig. 2 shows open-field performance and number of stools after 20 min. Fig. 2A indicates animal locomotion per 1-min block measured by mean number of beam crossing when two beams in each direction were positioned in 10-cm apart. The first 10 min was conducted in light, with the next 10 min in darkness. In general, crossing decreased as time passed during both lighting conditions. Mixed-type ANOVA including one between (group G) and two within-subject factors [light versus dark period (LD), and time in the session (T)] indicated that the main effect of T was significant [$F(9, 360) = 13.865$, $p < .0001$]. Interaction effects of T × G and LD × T were significant [$F(27, 360) = 1.949$, $p = .0037$ and $F(9, 360) = 7.517$, $p < .0001$, respectively]. However, main effects of G and LD and other interaction effects were not significant.

Fig. 2B presents mean number of rearing responses by 1-min block, measured as mean number of horizontal interruptions at 5 cm above the box floor. Mixed-type ANOVA showed that main effects of G, LD, and T all were significant [$F(3, 40) = 3.876$,

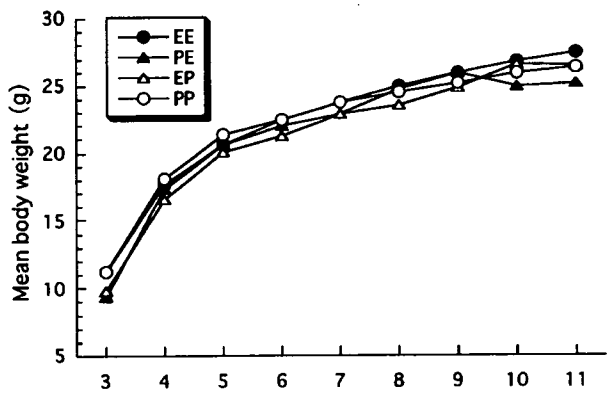


Fig. 1. Mean body weight change of four different housing groups from 3 to 11 weeks of age. Water and food were always available.

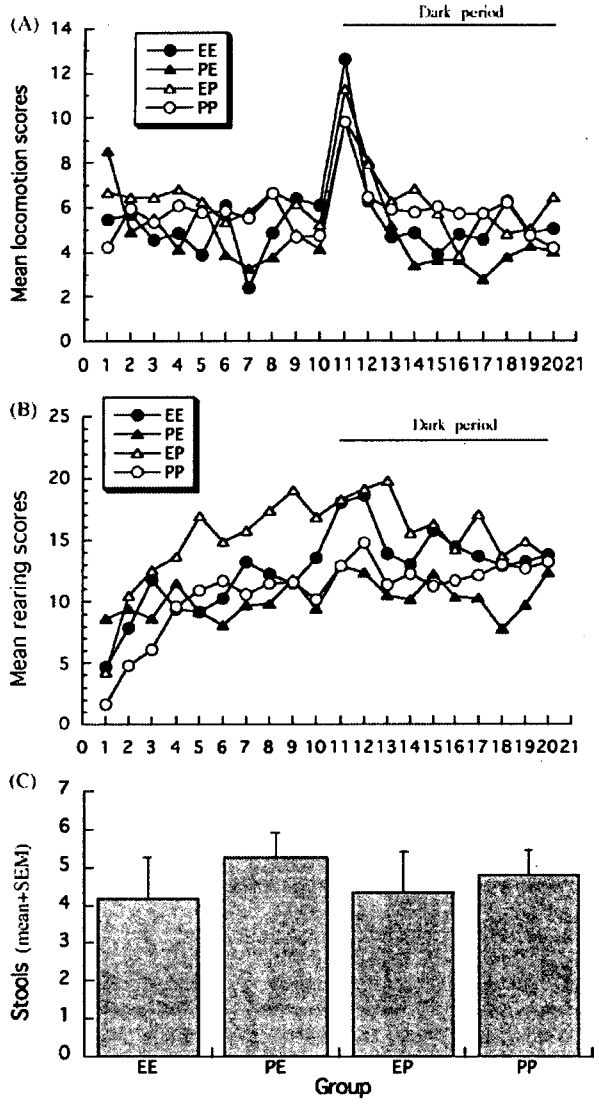


Fig. 2. Results of open-field test. Locomotion (A) counted by horizontal beam-cutting and rearing (B) measured by vertical beam-cutting were plotted. Ten minutes of light period were followed by 10 min of darkness, continuously. Stools found at the end of the session also were counted (C). All data are mean.

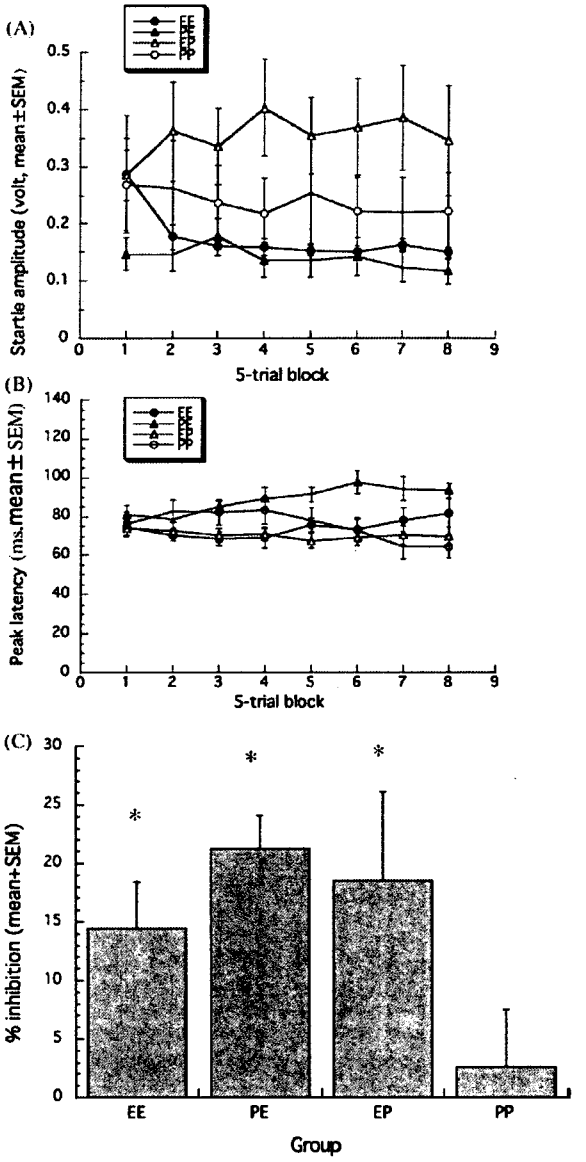


Fig. 3. Results for acoustic startle reflex and prepulse inhibition tests. Startle amplitude in volts (A), and peak latency during 40 trials of habituation (B) were plotted by 5-trial block, and prepulse inhibition by auditory prepulse with 50 ms of lead time (prepulse-pulse interval) condition (C) are shown. Asterisk shows significant inhibition. Data are mean ± SEM.

$p = .0159$; $F(1, 40) = 47.981$, $p < .0001$; $F(9, 360) = 3.682$, $p = .0002$, respectively]. Interaction effects of LD × G, T × G, LD × T, and LD × T × G were significant [$F(3, 40) = 2.937$, $p = .0448$; $F(27, 360) = 1.537$, $p = .0448$; $F(9, 360) = 17.048$, $p < .0001$; $F(27, 360) = 1.803$, $p = .0094$, respectively]. The group differences between EE and EP, EE and PE, EP and PE, and EP and PP were significant by the post hoc test.

Fig. 2C shows the mean number of stools per 20-min session. No group differences were observed [$F(3, 40) < 1$].

### 3.1.3. Startle reflex and prepulse inhibition

Fig. 3A shows mean amplitude of the auditory startle reflex in the 40 trials of the habituation period by 5-trial block. The results of mixed-type ANOVA indicated no main effects and the interaction effect were significant. Fig. 3B indicates mean peak latencies of the auditory startle reflex. Time to maximum movement amplitude in milliseconds after the start of the startle stimulus was recorded. Group EP showed shorter latency and group PE showed longer latency than the other groups. The results of the mixed-type ANOVA indicated that main effect of G and trial block (TB) [$F(3, 40) = 3.806$, $p = .0172$ and $F(7, 280) = 2.43$, $p = .0197$, respectively] and interactions of TB × G was significant [$F(21, 280) = 1.655$, $p = .0376$]. Fig. 3C shows mean percentage of prepulse inhibition under the auditory prepulse condition at a lead time of 50 ms, in which greatest inhibition was observed. Prepulse inhibition was smallest in the PP group, and inhibitions of the EE, PE and EP groups were significant ($Z = 3.48$, 2.43, and 6.92, respectively), but inhibition of PP mice was not ($Z = 0.53$).

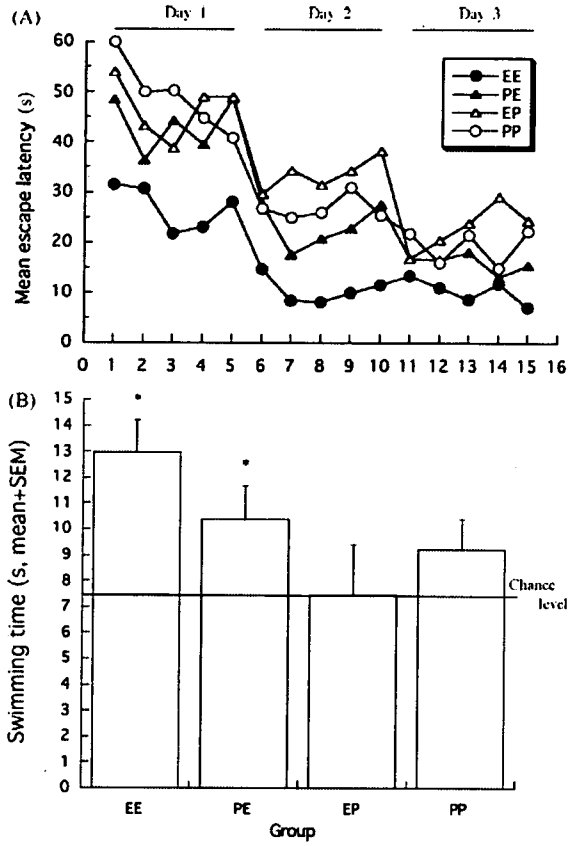


Fig. 4. Results for Morris water-maze learning. Mean latency of all trials in the three daily 5-trial sessions was plotted (A). The differences between EE and the other 3 groups, between PE and EP groups were significant. The results of probe test (B). Mice were allowed to search platform for 30 s. The mean of the total swimming time in the quadrant in which ever had contained the platform during training is shown. Asterisk shows significantly longer swimming time than chance level (7.5 s).

### 3.1.4. Water-maze learning

Fig. 4A shows mean water-maze latencies for all trials during three daily training sessions. From the first trial, EE mice performed better than other groups, reaching a plateau on the second training day. PP animals performed worst. The PE group showed learning curve intermediate between EE and PP groups. Results of mixed-type ANOVA including one between-subject factor (G) and two within-subject factors (day, D; trial, T) for water-maze learning showed that main effect of G and D were significant [$F(3, 40) = 7.637$, $p = .0004$ and $F(2, 80) = 65.883$, $p < .0001$, respectively]. Main effects of T [$F(4, 160) = 1.764$] and other interaction effects were not significant. The results of post hoc tests indicated group differences between EE and EP, EE and PE, EE and PP, and EP and PE were significant. Fig. 4B shows mean swimming time during 30 s probe test in the quadrant where the platform was placed during water-maze learning. Groups EE and PE showed significantly longer swimming time than the chance level (7.5 s) [$Z = 4.409$, $p < .01$ and $Z = 2.875$, $p < .01$, respectively], but the swimming time of groups PP and EP were not significantly different from the chance level [$Z = .03$ and 1.496, respectively]. Groups EE and PE were better at maze learning than the other two groups,

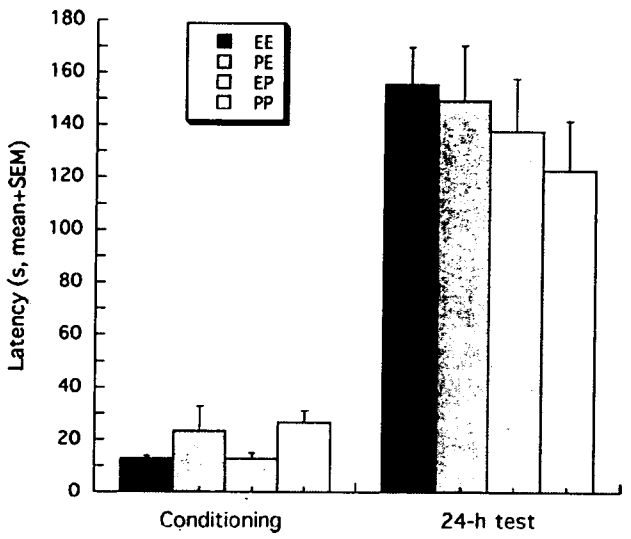


Fig. 5. The results of passive avoidance test. Step-through latencies from light to dark compartments in the conditioning trial (left) and the 24-h test trial (right) are plotted (mean + S.E.M.).

and memorized relatively well where the platform had been placed.

### 3.1.5. Passive avoidance

Fig. 5 shows mean step-through latencies in the conditioning and 24-h test trials of the passive avoidance test. Although PP mice showed longer latency than EE and EP groups during the conditioning trial, ANOVA performed including the respective trials indicated no group differences for conditioning or 24-h test trials [$F(3, 40) = 2.599$, $p = .065$ and $F(3, 40) < 1$, respectively].

## 3.2. Neuroanatomic data

### 3.2.1. Brain weight

Environmental change affected brain weight as well as behaviour. Fig. 6 shows mean weight of the brain determined after completion of all behavioural tests. Animals were 13 weeks old. EE and PE mice had heavier brains than PP and EP animals. ANOVA showed this group effect to be significant [$F(3, 34) = 3.288$, $p < .0323$]. Results of the group comparisons by post hoc tests indicated that group differences between EE and EP, EP and PE, and PE and PP were significant.

### 3.2.2. Induction of neuronal regeneration in situ

To examine the basis for increased brain weight in the enriched condition, generation of neuronal cells in cerebral cortex and hippocampus was assessed by *in vivo* BrdU labeling. Sections were visualised by confocal microscopy with antibody labeling for BrdU and PSA-NCAM. Cellular profiles for both markers were considered newly generated neurons (Fig. 7). Neuronal generation continued during the enriched condition, but decreased after 2 weeks in the impoverished condition. Newly generated neurons were present at a constant but low level in continuously impoverished (PP) mice.